ACS OMEGA

http://pubs.acs.org/journal/acsodf

Article

Lignin Residue-Derived Carbon-Supported Nanoscale Iron Catalyst for the Selective Hydrogenation of Nitroarenes and Aromatic Aldehydes

Naina Sarki, Raju Kumar, Baint Singh, Anjan Ray, Ganesh Naik, Kishore Natte,* and Anand Narani*

Cite This: *ACS Omega* 2022, 7, 19804−19815

Read Online

ACCESS | Metrics & More | Article Recommendations | Supporting Information

ABSTRACT: Heterogeneous iron-based catalysts governing selectivity for the reduction of nitroarenes and aldehydes have received tremendous attention in the arena of catalysis, but relatively less success has been achieved. Herein, we report a green strategy for the facile synthesis of a lignin residue-derived carbon-supported magnetic iron (γ-Fe_2O_3/LRC-700) nanocatalyst. This active nanocatalyst exhibits excellent activity and selectivity for the hydrogenation of nitroarenes to anilines, including pharmaceuticals (e.g., flutamide and nimesulide). Challenging and reducible functionalities such as halogens (e.g., chloro, iodo, and fluoro) and ketone, ester, and amide groups were tolerated. Moreover, biomass-derived aldehyde (e.g., furfural) and other aromatic aldehydes were also effective for the hydrogenation process, often useful in biomedical sciences and other important areas. Before and after the reaction, the γ-Fe_2O_3/LRC-700 nanocatalyst was thoroughly characterized by X-ray diffraction (XRD), N_2 adsorption−desorption, X-ray photoelectron spectroscopy (XPS), high-resolution transmission electron microscopy (HR-TEM), Raman spectroscopy, and thermogravimetric analysis (TGA). Additionally, the γ-Fe_2O_3/LRC-700 nanocatalyst is stable and easily separated using an external magnet and recycled up to five cycles with no substantial drop in the activity. Eventually, sustainable and green credentials for the hydrogenation reactions of 4-nitrobenzamide to 4-aminobenzamide and benzaldehyde to benzyl alcohol were assessed with the help of the CHEM21 green metrics toolkit.

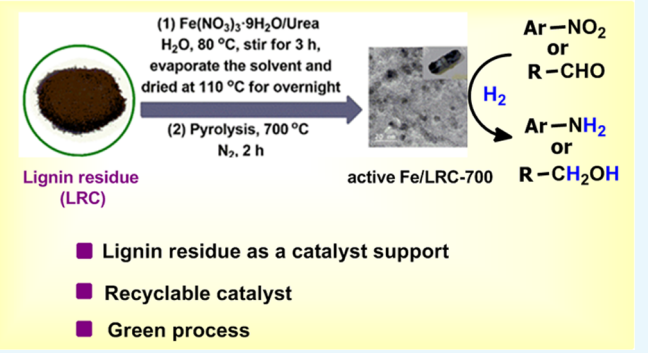

INTRODUCTION

Owing to the extensive application of aromatic amines and alcohols in everyday life (e.g., drugs, pesticides, fungicides, polyurethane, perfumes, etc.) and the chemical industry (e.g., fine and bulk chemicals), finding selective strategies for their synthesis by avoiding waste products continues to be scientifically attractive for a range of practical applications.[1−6] Over the last decade, chemists have devoted intense efforts to the development of both homogeneous and heterogeneous earth-abundant catalysts with enhanced catalytic properties that selectively give the desired products in high yields.[7−10] In particular, hydrogenation reactions with iron-based catalysts in the presence of molecular hydrogen have strongly boosted the catalysis research because iron is the most abundant element on the Earth, environmentally friendly, inexpensive, and non-toxic.[2,11,12] Its catalytic utility has also benefited some bioactive compound synthesis and materials science.[2,12] Hence, it is highly important to design iron catalysts and to promote them in clean and sustainable hydrogenation processes, aiming at chemical manufacturing with high efficiency and atom economy.[2,3,12]

Chemoselective hydrogenation of nitroarenes using molecular hydrogen in the presence of more reactive functional group entities represents an essential transformation in advanced organic synthesis since anilines serve as potential building blocks in numerous industrial domains.[2,4,13−16] In this respect, precious metals such as Rh, Pd, Au, and Ag metal-based catalysts have demonstrated outstanding catalytic activity for selective hydrogenation of functionalized nitroarenes.[2,4,13−15] However, a major drawback of employing these precious metals in industrial applications would be the high cost, limited availability, and accompanying safety, health, and sustainability considerations. In addition, the disposal of spent catalysts and effluent is also often a challenge. In the context of efforts to accomplish the Sustainable Development Goals (SDGs), novel catalysts based on earth-abundant metals with significant properties such as activity, selectivity, and recyclability are highly desired.[4] Within this context, in 2011 and 2013, Beller and co-workers exploded nanoscale cobalt-

Received: March 16, 2022
Accepted: May 20, 2022
Published: June 3, 2022

and iron-based catalysts for chemoselective hydrogenation of nitroarenes with various functional groups, including related hydrogenation reactions.[2,17] After their seminal work, several other research groups have shown increasing interest and extended the chemoselective hydrogenation of nitroarenes in the presence of 3d metals.[18−20] Despite their excellent catalytic performance, the synthesis of such nanostructured active materials requires expensive organic functional ligands and metal supports. In response to this issue, biomass-derived carbon-supported metal-based catalysts have engrossed strong interest owing to the porosity, high surface area, superior electron conductivity, and relative chemical resistance.[21−23] Some progress has been made on renewable carbon-supported metal-based catalysts to hydrogenate nitroarenes to anilines.[24−29] Recently, our group also exploited biomass-derived carbon-supported cobalt and ruthenium catalysts for selective hydrogenation reactions. This knowledge initiated the search for new sustainable and renewable carbon-rich sources as a catalyst support.[28−30]

On the other hand, the catalytic hydrogenation of aldehydes using molecular hydrogen is an environmentally benign and cost-effective method of obtaining useful alcohols to produce a wide range of fine and bulk chemicals, including surfactants and fragrance compounds, and others.[5,31−34] In the last few decades, a wide variety of noble[35,36] and non-noble-based[37−40] catalysts have been developed for these hydrogenation reactions. Concerning iron catalysis, homogeneous iron-based catalysts have shown excellent activity for the hydrogenation of aldehydes and ketones.[31] However, these homogeneous catalysts are difficult to separate and reuse. Surprisingly, the heterogeneous iron-based catalysts for such reduction with a broad substrate scope are absent. Hence, the development of an iron-based nanocatalyst for the chemoselective hydrogenation of aldehydes is highly desirable from the viewpoint of sustainability.

Motivating from the aforementioned reports and understanding the role of biomass utilization for the catalyst preparation, we chose lignin residue as an alternative carbon resource. Interestingly, there are few reports on the application of lignin-derived catalysts for organic transformations.[41] Typically, the bio-oil obtained from lignin decomposition is used to produce either aromatic chemicals[42] or upgraded to high-value-added products[43] including fuels.[44] During this process, unconverted lignin (stable solid with enriched carbon) is left over as a byproduct (lignin residue) and not used for potential applications. After considering this fact, we became interested in using this lignin residue as a metal support. The solid catalysts prepared from such residues obtained from the lignin represent an attractive property for lowering the carbon footprint. Recently, we have reported a lignin residue-derived carbon-supported Ni catalyst for selective hydrogenation of dehydrozingerone to zingerone.[45] In continuation of our scientific focus in the development of biomass/lignin-derived carbon-supported metal catalysts for organic transformations, we present here a simple method for preparing lignin residue-derived carbon-supported magnetically recoverable γ-Fe_2O_3 nanoparticles *via* impregnation, followed by pyrolysis under a N_2 environment. The catalyst promotes the hydrogenation of structurally challenging and functionally diverse nitroarenes including pharmaceuticals as well as aldehydes under industrially viable conditions. Most importantly, the catalyst is stable and magnetically recoverable as well as green credentials for the hydrogenation reactions of 4-nitrobenzamide to 4-aminobenzamide and benzaldehyde to benzyl alcohol were assessed with the help of the CHEM21 green metrics toolkit.

EXPERIMENTAL SECTION

Materials. $Fe(NO_2)_3{\cdot}9H_2O$ and urea were purchased from Sigma-Aldrich. All nitro and aldehyde chemicals were purchased from Sigma-Aldrich or TCI, India, and used without further purification. Soda lignin was received from Kuantum Papers Ltd (Chandigarh, India).

General Procedure for the Preparation of Lignin Residue. Lignin residue was prepared by the hydrothermal treatment of soda lignin. In a typical procedure, 4 g of soda lignin was added to 50 mL of distilled water in a 100 mL batch autoclave. Then, the autoclave was placed in an oil bath and increased the reaction temperature to 180 °C for 4 h with continuous stirring. After completion of the reaction, the reactor was allowed to cooled down to room temperature, and unconverted soda lignin was separated from bio-oil by simple filtration. The separated lignin residue was dried in an oven at 110 °C overnight.

General Procedure for the Preparation of a γ-Fe_2O_3/LRC-700 Nanocatalyst. In a typical procedure, the aqueous solution of $Fe(NO_2)_3{\cdot}9H_2O$ (217 mg) and urea (96 mg) mixture was added dropwise to 1 g of lignin residue. The resulting solution mixture was stirred for 3 h at 80 °C and successive water removal occurred upon heating. The resulting solid material was dried in an oven at 100 °C overnight, followed by pyrolysis at 700 °C under an inert atmosphere for 2 h at a 3 °C min^{-1} heating rate.

General Procedure for the Hydrogenation of Nitroarene. A 25 mL tubular batch autoclave reactor was loaded with 50 mg of γ-Fe_2O_3/LRC-700 nanocatalyst, 0.5 mmol of nitroarene, and a 10:1 mixture of THF and H_2O (2 mL). The reactor was firmly sealed and purged 3−4 times with nitrogen and hydrogen to remove any remaining air before being pressured with the required hydrogen pressure (35−50 bar), and the reaction mixture was stirred at 120 °C for a predetermined time (6−36 h). After the reaction was completed, the reactor was left to cool down to room temperature. The remainder of the hydrogen was then released. Then, the catalyst was separated by simple filtration and properly washed 2−3 times with 2 mL of ethyl acetate and 2 mL of ethanol solvents. Following the solvent evaporation using a rotary evaporator under vacuum, the crude product was subjected to column chromatography (hexane/EtOAc) to obtain the pure product, which was then submitted for GC−MS and NMR analyses.

General Procedure for the Hydrogenation of Aldehyde. All reactions were performed in a 25 mL tubular batch autoclave reactor. In brief, the reactor was loaded with 0.5 mmol of aromatic aldehyde in 2 mL of 10:1 mixture of THF solvent and 50 mg of γ-Fe_2O_3/LRC-700 nanocatalyst. Then, the reactor was well sealed and removed the air from the reactor by purging with nitrogen and hydrogen gases 3−4 times, and the reactor was filled with 35 bar H_2 pressure at ambient temperature. The reactor was then immersed in an oil bath at 120 °C with steady stirring for 18 h. After the reaction, the reactor temperature was brought down to room temperature by placing it in a water bath. The excess H_2 gas was gently and carefully expelled. Following that, the catalyst was simply filtered and washed 2−3 times with ethyl acetate and ethanol solvents. The desired pure product was obtained by

https://doi.org/10.1021/acsomega.2c01566
ACS Omega 2022, 7, 19804−19815

Scheme 1. Preparation of a Magnetically Recoverable Fe/LRC-700 Nanocatalyst

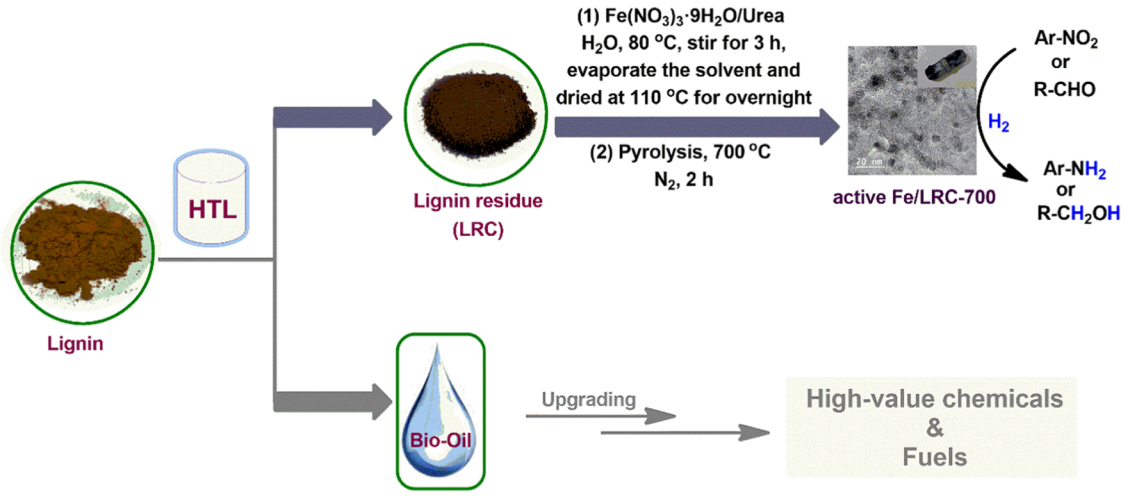

purifying the crude product mixture using column chromatography using a hexane/EtOAc eluent, which was then submitted for GC−MS and NMR analyses.

Procedure for Gram-Scale Reactions. A 25 mL tubular batch autoclave reactor was loaded with γ-Fe_2O_3/LRC-700 nanocatalyst (5 mol % Fe) and 4-(2-fluoro-4-nitrophenyl) morpholine (1 g, 4.43 mmol) or furfural (1.01 g, 10.41 mmol) in a 10:1 mixture of THF and H_2O (10 mL), and the reactor was tightly sealed. First, the air was removed by purging 3−4 times with nitrogen and hydrogen and then was pressurized with 35 bar H_2 and heated in an oil bath at 120 °C for 24 and 18 h in the case of 4-(2-fluoro-4-nitrophenyl) morpholine and furfural, respectively. After the completion of the reaction, the reactor was placed in a water bath to cool down, and the excess H_2 was carefully released, followed by filtration of the reaction mixture and separation of the catalyst. The obtained crude mixture was subjected to column chromatography using a hexane/EtOAc eluent to obtain the pure product and submitted for GC−MS and NMR analyses.

RESULTS AND DISCUSSION

Synthesis of the Catalyst. In the beginning of the work, the lignin residue-derived carbon-supported magnetic iron nanocatalyst was synthesized by the hydrothermal treatment of lignin, followed by impregnation and subsequent pyrolysis. Soda lignin was hydrothermally treated to yield the bio-oil and lignin residue (unconverted lignin). Then, the obtained lignin residue was impregnated with an aqueous solution of $Fe(NO_2)_3{\cdot}9H_2O$ and urea at 80 °C for 3 h, after which the surplus water solvent was removed, and the material was dried. The dry materials were pyrolyzed for 2 h at 700 °C in a N_2 environment (Scheme 1). At last, the resultant black material was designated as Fe/LRC-700.

Catalyst Characterization. To understand the exceptional catalytic activity of the magnetic Fe/LRC-700 nanocatalyst, we characterized the catalyst by comprehensive analytical techniques, including CHNS, ICP-AES, powder XRD, N_2 adsorption−desorption, XPS, HR-TEM, Raman, and TGA analyses. According to elemental (CHNS) analysis, the Fe/LRC-700 nanocatalyst has 80% carbon, 2.2% hydrogen, 1.2% nitrogen, and 16.6% oxygen. The Fe content in the catalyst is estimated to be around 2.8 wt % Fe by ICP-AES analysis. The powder XRD patterns of fresh and spent Fe/LRC-700 nanocatalysts are shown in Figure 1. The fresh Fe/LRC-700 nanocatalyst exhibited the diffraction peaks on the 2-θ scale at

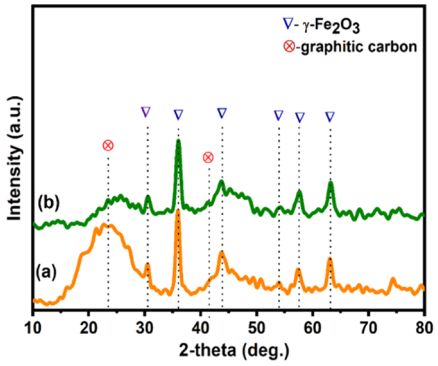

Figure 1. XRD pattern of the Fe/LRC-700 nanocatalyst (a) before and (b) after the reaction.

30.63, 35.88, 43.63, 53.88, 57.50, and 63.18° that are associated with the (220), (311), (400),(422), (511), and (440) planes of a magnetic maghemite γ-Fe_2O_3 phase with a cubic structure (JCPDS file 39-1346), respectively.[46,47] Furthermore, a broad diffraction peak appeared at 24° and the peak around 42° corresponding to the (002) and (100) planes of carbon with amorphous nature.[28] After the reaction, no substantial change in the diffraction pattern of the Fe/LRC-700 nanocatalyst was observed, indicating the retention of the maghemite γ-Fe_2O_3 phase in the used catalyst. The N_2 adsorption−desorption analysis was studied to examine the structural and textural characteristics of the Fe/LRC-700 nanocatalyst, and the corresponding isotherm is shown in Figure 2. The catalyst exhibits type-IV isotherm with a hysteresis loop, suggesting the mesopores in the catalyst, with pores ranging in size from 2 to 3.5 nm. The Fe/LRC-700 nanocatalyst has a BET surface area of 160 m^2/g and a total pore volume of 0.013 cm^3/g.

X-ray photoelectron spectroscopy (XPS) was used to identify the chemical oxidation states of elements present in the Fe/LRC-700 nanocatalyst, and the corresponding images are displayed in Figure 3. The survey XPS spectrum confirms the presence of iron (Fe), nitrogen (N), carbon (C), and oxygen (O) elements in the Fe/LRC-700 nanocatalyst (see the Supporting Information, Figure S1). The deconvoluted N 1s

https://doi.org/10.1021/acsomega.2c01566
ACS Omega 2022, 7, 19804−19815

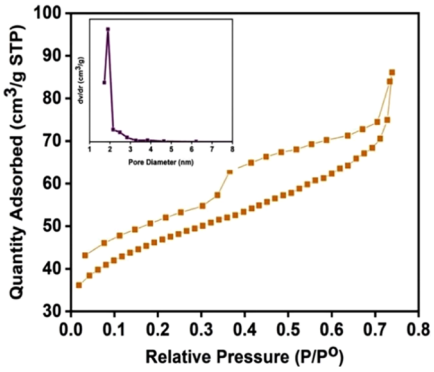

Figure 2. N_2 adsorption−desorption isotherms of the Fe/LRC-700 nanocatalyst. Inset: pore size distribution curve.

spectra (Figure 3a) can be fitted into three prominent peaks. Pyridinic nitrogen is responsible for the energy band at 398.9 eV. On the other hand, the energy band at 400.3 eV is attributed to graphitic nitrogen, which is formed by substituting carbon atoms with nitrogen on the edges or defects in the graphene sheets. This finding suggests that the nitrogen atoms from the urea source were transformed into pyridinic and graphitic nitrogen, confirming the formation of N-doped carbon material during pyrolysis. The binding energy at 406.4 eV corresponds to oxidized nitrogen atoms (N-oxides) present in the Fe/LRC-700 nanocatalyst.[48,49] Further, we also noticed that nitrogen could also exist in the carbon shells encapsulating Fe nanoparticles. The mathematically deconvoluted XPS spectrum of Fe 2p is displayed in Figure 3b. The energy bands centered at 712.01 and 725.12 eV match with Fe $2p_{3/2}$ and Fe $2p_{1/2}$ of iron in +3 oxidation state (Fe^{+3}) of γ-Fe_2O_3. However, the binding energies are slightly higher than the reported values, suggesting a strong interaction between N atoms and Fe nanoparticles. Furthermore, the binding energies at 718.81 and 732.82 eV correspond to charge transfer satellite peaks of Fe $2p_{3/2}$ and Fe $2p_{1/2}$, providing strong support for the formation of γ-Fe_2O_3 in the Fe/LRC-700 nanocatalyst. These observations are well matched with the findings in XRD and previous reports.[50−52] The high-resolution C 1s XPS spectrum of the Fe/LRC-700 nanocatalyst (Figure 3c) demonstrates that the carbon is in four different chemical environments. The major peak visualized at 284.77 eV can be allocated to sp^2-hybridized conjugated graphite-like carbon (C−Csp^2). The broad peak centered at 286.25 eV could be attributed to sp^3-hybridized carbon (C−Csp^3), which overlaps with the carbon attached to nitrogen (N−Csp^2). The sp^3-hybridized carbon originates from the defects present in the graphite structure. In addition, two other deconvoluted peaks appeared at 288.89 and 292.75 eV were allocated to −C═O and $\pi-\pi^*$ transitions in a graphitic structure, respectively.[20] The O 1s core-level XPS spectra of the Fe/LRC-700 nanocatalyst (Figure 3d) showed two peaks at 532.09 and 533.80 eV due to −C═O and −O−CO/C−OH

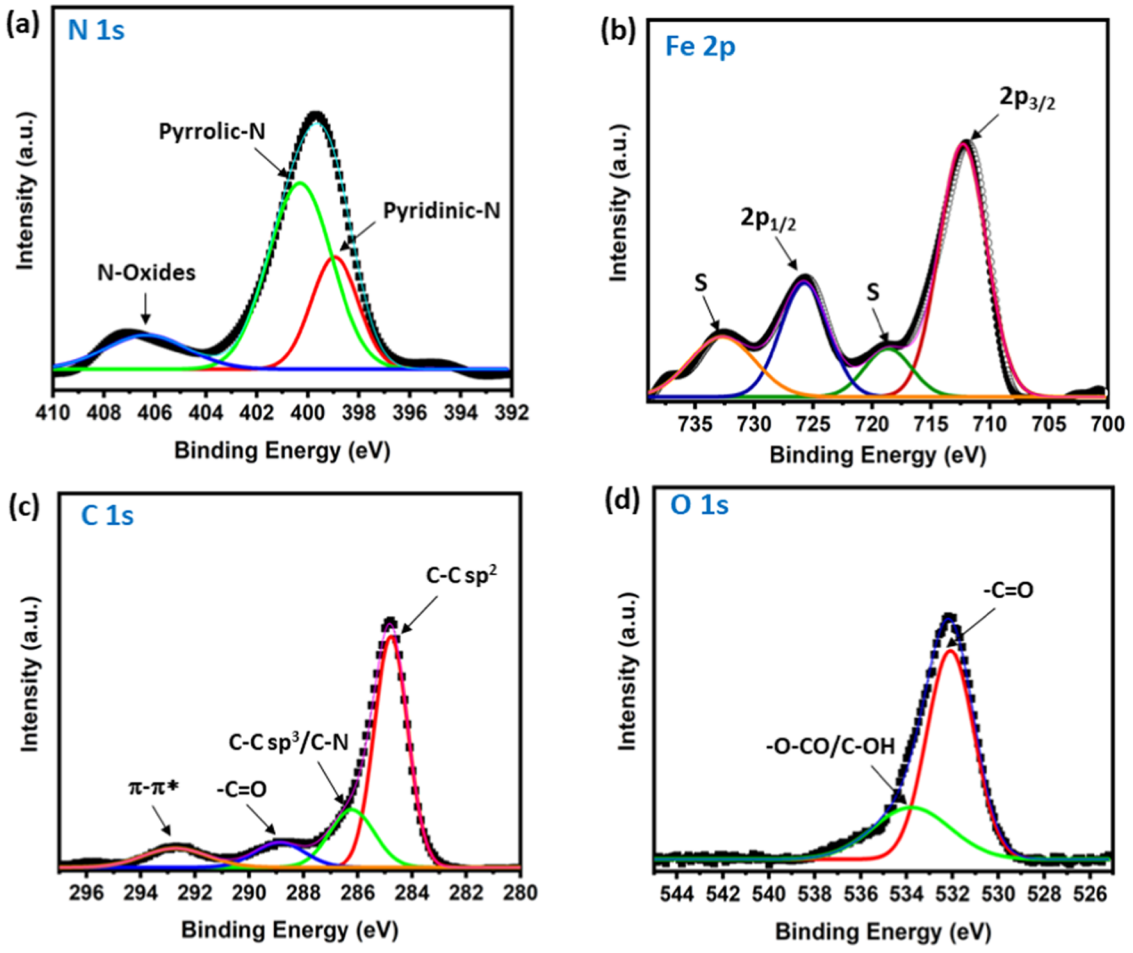

Figure 3. XPS spectra of the Fe/LRC-700 nanocatalyst: (a) N 1s, (b) Fe 2p, (c) C 1s, and (d) O 1s spectra.

https://doi.org/10.1021/acsomega.2c01566
ACS Omega 2022, 7, 19804−19815

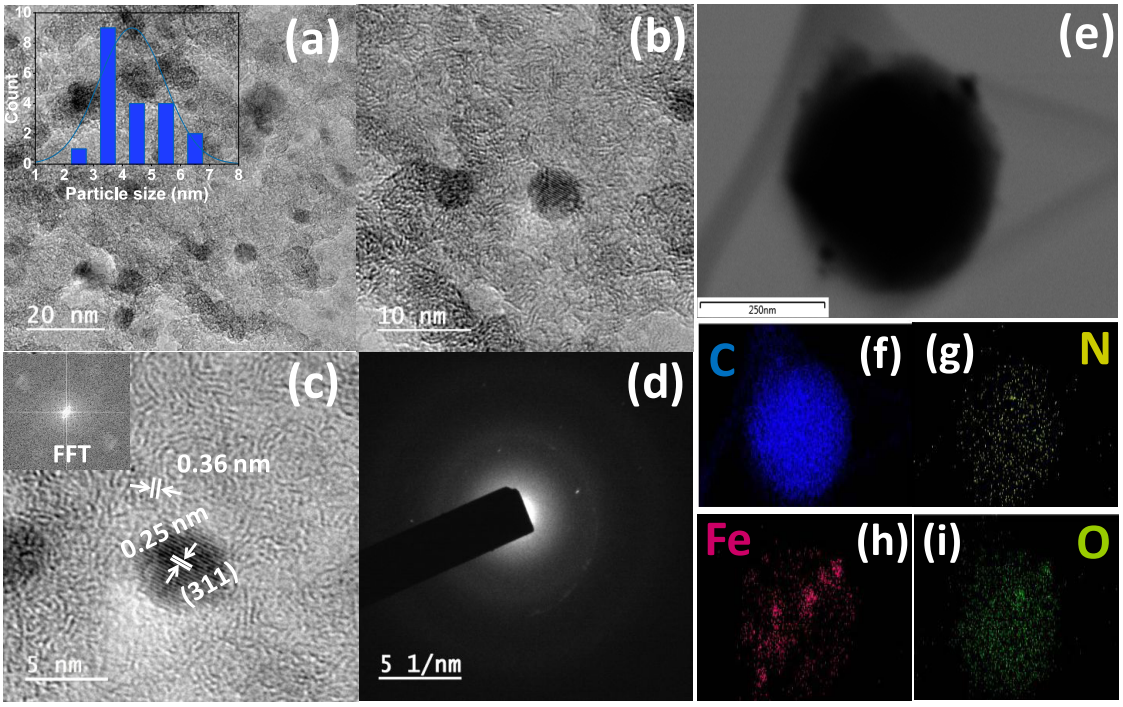

Figure 4. TEM images of the Fe/LRC-700 nanocatalyst: (a, b) TEM images of the Fe/LRC-700 nanocatalyst and nanoparticle distribution (inset), (c) HR-TEM image, (d) selected area electron diffraction (SAED) pattern, and (e–i) elemental mapping patterns (Fe, C, N, O) of the Fe/LRC-700 nanocatalyst.

bonds.[53] After the reaction, no change in chemical oxidation states of Fe, N, C, and O species was observed in the Fe/LRC-700 nanocatalyst (see the Supporting Information, Figures S2 and S3).

The TEM images of the Fe/LRC-700 nanocatalyst are shown in Figure 4, demonstrating that Fe nanoparticles are spherical and have a size ranging from 2 to 7 nm (Figure 4a,b) with a mean diameter of 4.34 nm. Besides, Fe nanoparticles are evenly distributed throughout the graphitic carbon material. The HR-TEM images of Fe/LRC-700 in Figure 4c reveal that the lattice fringe spacing of 0.25 nm corresponds to the lattice plane distance (d) value of the (311) crystal plane of the maghemite γ-Fe_2O_3 phase[50] and is consistent with XRD and XPS results. In addition, the d value of 0.36 nm represents the (002) crystal plane of graphitic carbon. Figure 4d shows the selected area diffraction (SAED) profile of the Fe/LRC-700 nanocatalyst, revealing the amorphous nature of the γ-Fe_2O_3 nanoparticles with diffused rings. An energy-dispersive X-ray (EDX) study of the Fe/LRC-700 nanocatalyst (Figure 4e–i) shows that elements of iron, nitrogen, carbon, and oxygen species overlap in the catalyst material.

The Raman analysis of the Fe/LRC-700 nanocatalyst before and after the reaction was investigated, and the representative spectra are shown in Figure 5. Both fresh and used Fe/LRC-700 nanocatalysts exhibit two Raman bands at 1332 and 1594 cm^{-1}, corresponding to the D (A_{1g}) and G (E_{2g}) bands, respectively (Figure 5a,b). The Raman D-band is produced due to out-of-plane vibrations, which indicate structural flaws in the catalyst, whereas the Raman G-band is a characteristic feature of a graphitic structure of the catalyst.[54] The D and G band ratios (I_D/I_G) in carbon materials determine the defect density in the D and G band ratios. The I_D/I_G of fresh and used Fe/LRC-700 nanocatalysts is about 1.9 and 2.0, indicating that a graphitic structure with structural flaws is

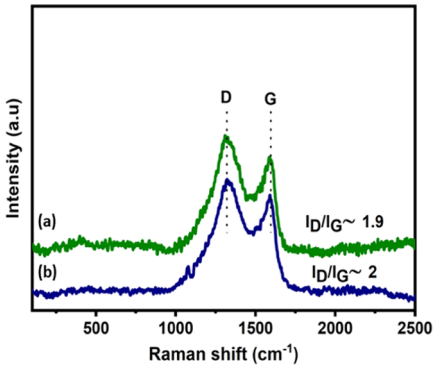

Figure 5. Raman spectra of the Fe/LRC-700 nanocatalyst: (a) before the reaction and (b) after the reaction.

present in both catalysts.[49] Therefore, the Raman analysis reveals no changes in the Fe/LRC-700 nanocatalyst structure after the reaction.

A thermogravimetric analysis (TGA) study was used to assess the thermal stability of the Fe/LRC-700 nanocatalyst. As illustrated in Figure 6, the 5.5 wt % mass loss observed around 100 °C is attributable to the loss of water molecules adsorbed on the catalyst surface. The Fe/LRC-700 nanocatalyst is stable up to 270 °C; beyond this temperature, an evident mass loss (22 wt %) was monitored, attributed to the decomposition of the carbon support.

The XRD, XPS, and HR-TEM analyses confirm the maghemite γ-Fe_2O_3 phase formation in the Fe/LRC-700 nanocatalyst. Hence, the catalyst is designated as the γ-Fe_2O_3/LRC-700 nanocatalyst.

Catalyst Screening. The catalytic activity of the γ-Fe_2O_3/LRC-700 nanocatalyst was evaluated for the selective hydrogenation of industrially relevant benchmark substrate 4-

https://doi.org/10.1021/acsomega.2c01566
ACS Omega 2022, 7, 19804−19815

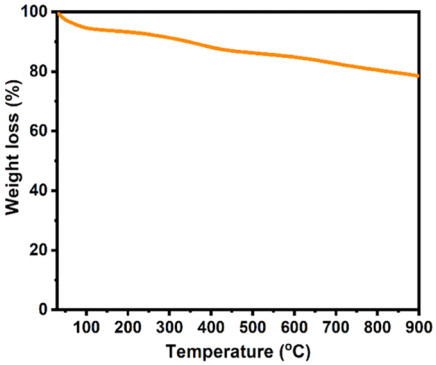

Figure 6. Thermogravimetric analysis of the Fe/LRC-700 nanocatalyst.

nitrochlorobenzene with molecular hydrogen. This model reaction allows us to monitor the overall selectivity of the nitro group hydrogenation over C−Cl (dechlorination). Because chloronitroarenes are very sensitive to the molecular hydrogen,[28] achieving high selectivity is one of the main challenges in this chemistry. Initially, the reaction was carried out without a catalyst, and no progress was observed. (Table 1, entry 1). We then investigated lignin residue (LR), lignin residue-derived carbon (LRC), and $Fe_2(NO_3)_2{\cdot}9H_2O$ for the production of the desired 4-chloroaniline and observed that all of these materials are completely inactive (Table 1, entries 2−4). The catalytic activity of $Fe_2(NO_3)_2{\cdot}9H_2O$/LR and $Fe_2(NO_3)_2{\cdot}9H_2O$/LRC catalysts was found to be very poor (Table 1, entries 5 and 6). The catalysts prepared and pyrolyzed at temperatures of 600 °C and 800 °C showed significant activity (Table 1, entries 7 and 9). Astonishingly, excellent conversion and selectivity were obtained with the γ-Fe_2O_3/LRC-700 nanocatalyst under 35 bar H_2 pressure at 120 °C for 18 h (Table 1, entry 8). The product 4-chloroaniline was isolated in quantitative yields (96%). The remarkable catalytic activity of the γ-Fe_2O_3/LRC-700 nanocatalyst for the selective hydrogenation of nitroaromatics is due to the strong interaction between N atoms and Fe nanoparticles, which could prevent aggregation of γ-Fe_2O_3 nanoparticles and, therefore, its activity.

Effect of Reaction Parameters. Since the γ-Fe_2O_3/LRC-700 nanocatalyst demonstrated exceptional activity and selectivity for the reduction of 4-nitrochlorobenzene to 4-chloroaniline (Table 1, entry 8), it was chosen to investigate the effects of reaction parameters, such as temperature, time, and H_2 pressure on 4-nitrochlorobenzene conversion and 4-chloroaniline selectivity. After having an active γ-Fe_2O_3/LRC-700 nanocatalyst in hand, the effect of reaction temperature and time on 4-nitrochlorobenzene conversion and 4-chloroaniline selectivity was investigated (Table 2, entries 1−6). The temperature is one of the vital reaction parameters that can affect the rate of conversion and selectivity. The reaction was carried out at different temperatures ranging from 30 to 120 °C, and the findings are presented in Table 2. As the temperature increases, so does the rate of 4-nitrochlorobenzene conversion. Only 5% of 4-nitrochlorobenzene conversion was obtained at 30 °C (Table 2, entry 1). By increasing the reaction temperature to 60 °C, the conversion was marginally increased (40%) and reached 70% at 90 °C (Table 2, entries 2 and 3). Further increasing the reaction temperature to 120 °C, a significant increase in conversion was observed and achieved 99% conversion and 99% selectivity (Table 2, entry 4). After that, we assessed the influence of reaction time on 4-nitrochlorobenzene conversion and 4-chloroaniline selectivity (Table 2, entries 5 and 6). The data shows an increase in 4-nitrochlorobenzene conversion as the reaction time progresses. The maximum conversion was reached after 18 h of reaction time. Further, the effect of H_2 pressure on 4-nitrochlorobenzene conversion and 4-chloroaniline selectivity was

Table 2. Effect of Temperature and Time on the Conversion and Selectivity of 4-Nitrochlorobenzene and 4-Chloroaniline over the γ-Fe_2O_3/LRC-700 Nanocatalyst[a]

entry	temperature (°C)	time (h)	4-nitrochlorobenzene conversion (%)	4-chloroaniline selectivity (%)
1	30	18	5	99
2	60	18	40	99
3	90	18	70	99
4	120	18	99	99
5	120	6	42	99
6	120	12	70	99

[a]Reaction conditions: 4-nitrochlorobenzene (0.5 mmol), γ-Fe_2O_3/LRC-700 nanocatalyst (50 mg, 5 mol % Fe), H_2 (35 bar), THF/H_2O (10:1); conversion and selectivity were determined by GC−MS.

Table 1. Hydrogenation of 4-Nitrochlorobenzene over Different Catalysts[a]

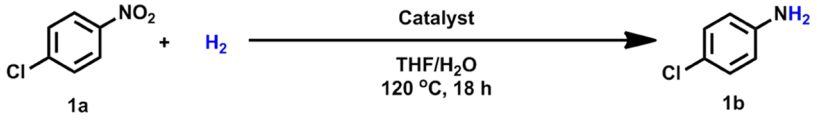

1a 1b

entry	catalyst	1a conversion (%)	1b selectivity (%)
1	without catalyst	n.d.	n.d.
2	lignin residue (LR)	n.d.	n.d.
3	lignin residue carbon (LRC)	n.d.	n.d.
4	$Fe_2(NO_3)_2{\cdot}9H_2O$	n.d.	n.d.
5	$Fe_2(NO_3)_2{\cdot}9H_2O$/LR	5	64
6	$Fe_2(NO_3)_2{\cdot}9H_2O$/LRC	10	80
7	γ-Fe_2O_3/LRC-600	87	99
8	γ-Fe_2O_3/LRC-700	99	99 (96)
9	γ-Fe_2O_3/LRC-800	90	95 (87)

[a]Reaction conditions: 0.5 mmol of **1a**, 50 mg of catalyst, 35 bar H_2, 2 mL of THF/H_2O (10:1), 120 °C, and 18 h; conversion and selectivity were determined with GC−MS; isolated yields by column chromatography shown in parenthesis.

https://doi.org/10.1021/acsomega.2c01566
ACS Omega 2022, 7, 19804−19815

inspected (Figure 7). The 4-nitrochlorobenzene conversion was steadily enhanced by increasing the H_2 pressure until it reached 99% at 35 bar H_2 pressure. The 4-chloroaniline selectivity remained constant over a range of reaction temperatures, times, and H_2 pressure. Hence, we found that the highest 4-nitrochlorobenzene conversion (99%) and 4-chloroaniline selectivity (99%) are achieved at 120 °C using 35 bar H_2 pressure for 18 h.

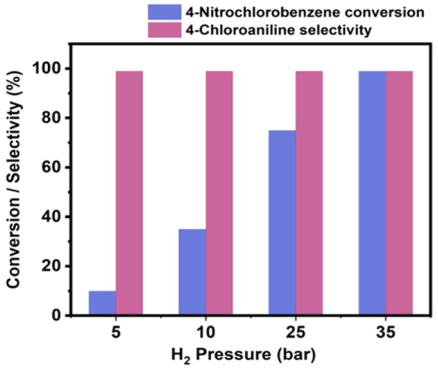

Figure 7. Effect of H_2 pressure on the conversion and selectivity of 4-nitrochlorobenzene and 4-chloroaniline over the γ-Fe_2O_3/LRC nanocatalyst (reaction conditions: 4-nitrochlorobenzene (0.5 mmol), γ-Fe_2O_3/LRC-700 nanocatalyst (50 mg, 5 mol % Fe), THF/H_2O (10:1), 120 °C, 18 h).

Catalytic Performance of γ-Fe_2O_3/LRC-700 Nanocatalyst for Chemoselective Hydrogenation of Nitroarenes. Using the optimized reaction conditions, we evaluated the scope of diverse nitroarenes in the presence of our novel γ-Fe_2O_3/LRC-700 nanocatalyst. A simple nitrobenzene was fully converted and gave the desired aniline in 95% yield (Scheme 2, entry 1). Hydrogenation of halonitroarenes to yield corresponding haloanilines is highly important because haloanilines are having enormous applications in dyes, agrochemicals, drugs, and polymers.[55] The major issue in the hydrogenation process of the nitro group is the hydrodehalogenation of haloanilines with molecular hydrogen. Gratifyingly, our iron catalyst tolerated chloro, iodo, and fluoro entities at different positions on the nitroarene substrates (Scheme 2, entries 2–8), providing the corresponding haloanilines in very good to

Scheme 2. Catalytic Performance of γ-Fe_2O_3/LRC-700 Nanocatalyst for Chemoselective Hydrogenation of Nitroarenes[a]

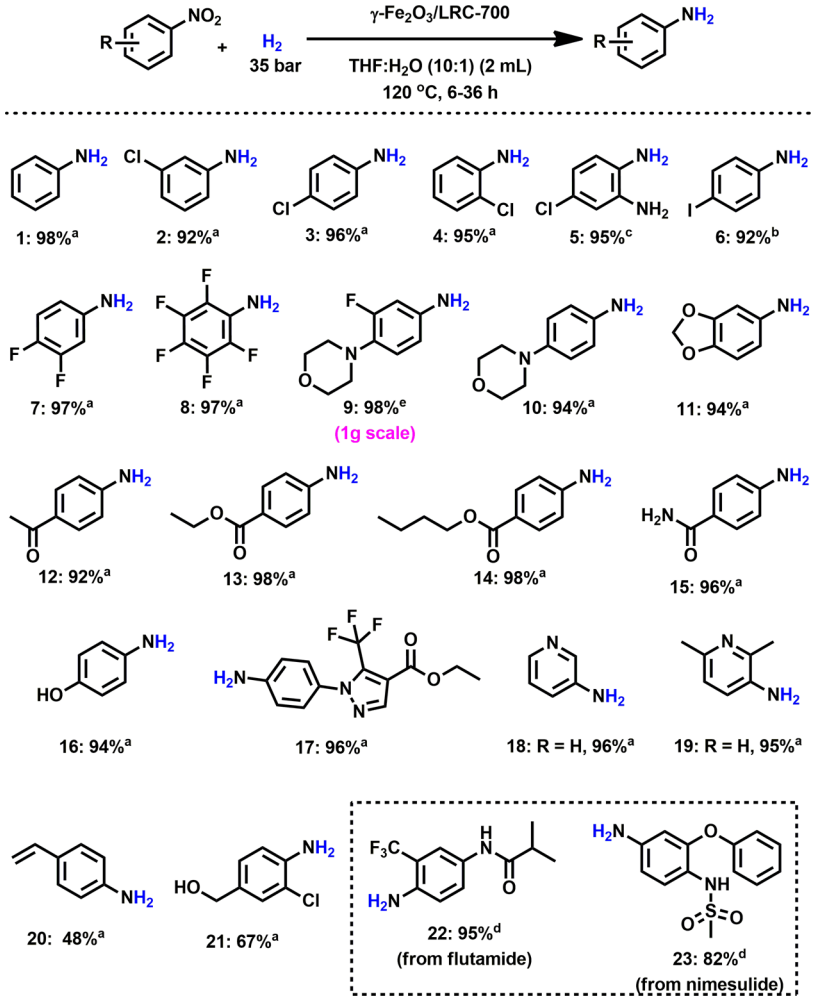

[a]Reaction conditions: [a] nitroarene (0.5 mmol), γ-Fe_2O_3/LRC-700 nanocatalyst (50 mg, 5 mol % Fe), H_2 (35 bar), THF/H_2O (10:1) (2 mL), 120 °C, 18 h. [b] Same as [a] with reaction time 6 h. [c] Same as [a] with reaction time 24 h. [d] Same as [a] with H_2 (50 bar) and reaction time 36 h. [e] 4-(2-Fluoro-4-nitrophenyl) morpholine (4.42 mmol), γ-Fe_2O_3/LRC-700 nanocatalyst (411 mg, 5 mol % Fe), H_2 (35 bar), THF/H_2O (10:1) (10 mL), 120 °C, 24 h.

https://doi.org/10.1021/acsomega.2c01566
ACS Omega 2022, 7, 19804−19815

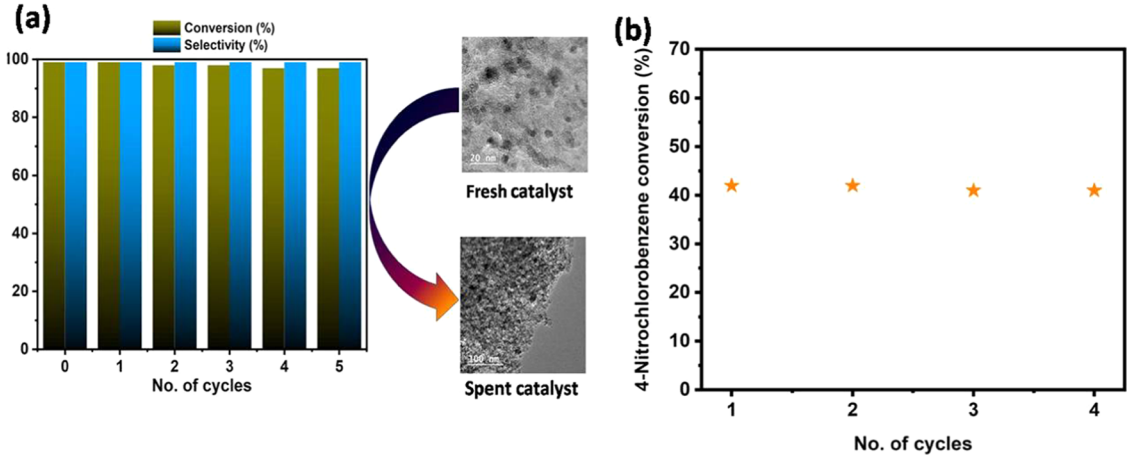

Figure 8. (a) Recyclability of the γ-Fe_2O_3/LRC-700 nanocatalyst. Reaction conditions: 4-nitrochlorobenzene (0.5 mmol), γ-Fe_2O_3/LRC-700 nanocatalyst (50 mg, 5 mol % Fe), H_2 (35 bar), THF/H_2O (10:1), 120 °C, and 18 h; GC−MS yields. (b) Stability of the γ-Fe_2O_3/LRC-700 nanocatalyst for the hydrogenation of 4-nitrochlorobenzene. Reaction conditions: 4-nitrochlorobenzene (0.5 mmol), γ-Fe_2O_3/LRC-700 nanocatalyst (50 mg, 5 mol % Fe), H_2 (35 bar), THF/H_2O (10:1), 120 °C, and 6 h; GC−MS yields.

Scheme 3. Catalytic Performance of γ-Fe_2O_3/LRC-700 Nanocatalyst for Selective Hydrogenation of Aromatic Aldehydes[a]

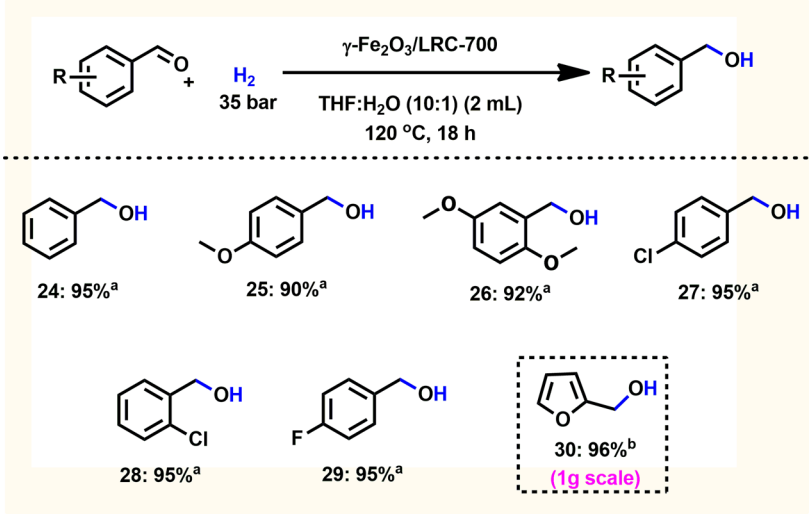

[a]Reaction conditions: aromatic aldehyde (0.5 mmol), γ-Fe_2O_3/LRC-700 nanocatalyst (50 mg, 5 mol % Fe), H_2 (35 bar), THF/H_2O (10:1) (2 mL), 120 °C, 18 h. [b]For gram-scale reaction: furfural (10.41 mmol), γ-Fe_2O_3/LRC-700 nanocatalyst (968 mg, 5 mol % Fe), H_2 (35 bar), THF/H_2O (10:1) (10 mL), 120 °C, 18 h.

excellent yields. Interestingly, the γ-Fe_2O_3/LRC-700 nanocatalyst is suitable for the gram-scale synthesis of a key pharmaceutical intermediate of a commercially important drug linezolid (Scheme 2, entry 9). In addition, 4-(4-nitrophenyl)-morpholine and 1,2-(methylenedioxy)-4-nitrobenzene were hugely effective in forming their corresponding anilines in 94% yield (Scheme 2, entries 10 and 11). Nitroarenes bearing electron-withdrawing groups gave quantitative conversion with excellent isolated yields (Scheme 2, entries 12−16). Notably, heterocyclic nitroarenes were compatible with the catalytic system affording the respective anilines in excellent isolated yields (Scheme 2, entries 17−19). Also, nitroarene containing reducible functional groups like alkene were tolerated and gave the corresponding aniline in moderate yield and double bond reduced aniline in comparable yield (Scheme 2, entry 20). However, when 3-chloro-4-nitrobenzaldehyde was employed as a starting material, along with the nitro moiety, reduction of the aldehyde group was also observed, and 4-amino-3-chloro benzyl alcohol was obtained in good yields (Scheme 2, entry 21). The high compatibility of this iron-catalyzed chemoselective hydrogenation of the nitro group encouraged us to examine its utility for late-stage reduction of pharmaceuticals. Flutamide, a nonsteroidal antiandrogen, and nimesulide, a nonsteroidal anti-inflammatory drug (NSAID), were selectively hydrogenated and afforded the respective anilines in very good yields (Scheme 2, entries 22 and 23).

Catalyst Stability and Recyclability. A hot filtration experiment was carried out for the hydrogenation of 4-nitrochlorobenzene for 10 h under optimized reaction conditions (0.5 mmol of 4-nitrochlorobenzene, 50 mg of γ-Fe_2O_3/LRC-700 nanocatalyst, H_2 (35 bar), THF/H_2O (10:1), 120 °C) to confirm the absence of leaching of Fe nanoparticles from the γ-Fe_2O_3/LRC-700 nanocatalyst. The catalyst was recovered from the reaction mixture by hot filtering after 10 h. The reaction was then proceeded by adding 0.5 mmol of 4-nitrochlorobenzene to the filtrate. No additional hydro-

https://doi.org/10.1021/acsomega.2c01566
ACS Omega 2022, 7, 19804−19815

Table 3. Zero Pass CHEM21 Green Metrics Toolkit for Selective Hydrogenation of 4-Nitrobenzamide (A) and Benzaldehyde (B)

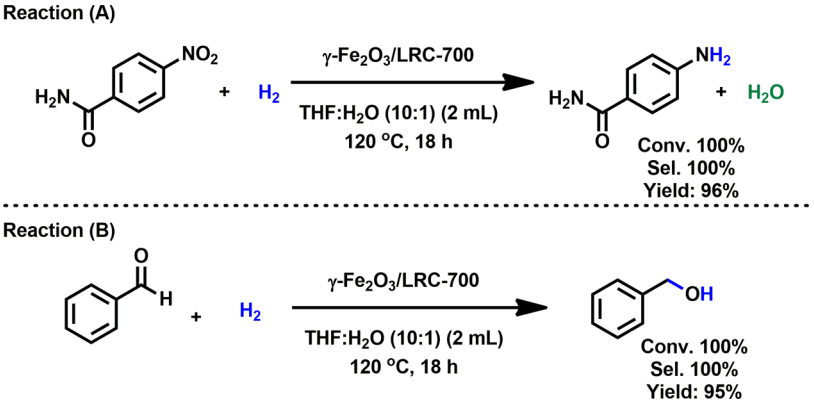

Metric	Reaction (A)	Reaction (B)
Yield	96	95
Conversion	100	100
Selectivity	100	100
Atom economy	79.09	100
Reaction mass efficiency	75.58	95.00
Solvent	THF, H_2O	THF, H_2O
Catalyst	Yes	Yes
Element	Fe	Fe
Reactor	Batch	Batch
Work up	Filtration	Filtration
Energy	120 °C	120 °C
Health and Safety	H280	H280

genation of 4-nitrochlorobenzene was detected, indicating that no Fe nanoparticles were leached into the solution mixture throughout the process. Furthermore, the filtrate was subjected to ICP-AES analysis, which revealed no evidence of Fe nanoparticles in the solution. Next, we have investigated the recyclability and reusability of the γ-Fe_2O_3/LRC-700 nanocatalyst under standard reaction conditions, and the corresponding results are shown in Figure 8a. After completion of the reaction, the catalyst was recovered by simple magnetic separation and washed several times with ethyl acetate and ethanol solvents. Then, the separated catalyst was dried at 60 °C under vacuum and reused five times. No considerable drop in catalytic activity and selectivity was observed even after the fifth catalytic cycle. Further, we have also assessed the stability of the γ-Fe_2O_3/LRC-700 nanocatalyst by recovering the catalyst and carried out the hydrogenation experiment for the conversion of 4-nitrochlorobenzene to 4-chloroaniline for a shorter reaction period (6 h), and the corresponding results are shown in Figure 8b. After 6 h of reaction time, 42% of 4-nitrochlorobenzene conversion was observed. No significant change in conversion was monitored in consecutive catalytic cycles, suggesting that the γ-Fe_2O_3/LRC-700 nanocatalyst is highly stable under the reaction conditions. No significant structural and morphological changes were noticed in the spent γ-Fe_2O_3/LRC-700 nanocatalyst (Figure 8a), but an aggregation of γ-Fe_2O_3 nanoparticles was realized. However, the catalytic activity of the γ-Fe_2O_3/LRC-700 nanocatalyst remained the same even after the fifth catalytic cycle.

Catalytic Performance of γ-Fe_2O_3/LRC-700 Nanocatalyst for Selective Hydrogenation of Aromatic Aldehydes. Subsequently, the synthesis of aromatic alcohols from the corresponding aldehydes was explored. Iron-catalyzed hydrogenation of aldehydes is scarcely reported in the literature. In general, aromatic alcohols are excellent starting materials in organic synthesis and have potential applications in chemical industries. The successful reduction of both nitro and aldehyde groups present in 3-chloro-4-nitrobenzaldehyde (Scheme 2, entry 21) motivated us to apply our γ-Fe_2O_3/LRC-700 nanocatalyst for the hydrogenation of aldehydes. Benzaldehyde was fully converted and gave the corresponding benzyl alcohol product in 95% yield (Scheme 3, entry 24). An aldehyde with an electron-rich substituent, for example, methoxy, afforded the corresponding alcohols in good yields (Scheme 3, entries 25 and 26). Halogen-containing aryl aldehydes did not seem to hinder the reduction rate, as shown by the similarity of the results, and gave the desired alcohols in excellent yields (Scheme 3, entries 27−29). The presence of the halogen group at the ortho position also did not affect the selectivity of the required alcohol product (Scheme 3, entry 28). Over the last few years, the hydrogenation of bio-based precursors to high-value-added chemicals has been significantly growing in biomass conversion strategies.[56] Among these, furfural hydrogenation to furfuryl alcohol is gaining huge attention owing to its commercial interest in several industries. Almost 62% of the furfural generated today is converted into furfuryl alcohol, which is mostly employed as a copper chromate catalyst in industrial processes.[57] Interestingly, applying our novel γ-Fe_2O_3/LRC-700 nanocatalyst, 1 g of furfural was selectively hydrogenated to furfuryl alcohol in 96% yield (Scheme 3, entry 30). Unfortunately, few aliphatic aldehydes did not undergo hydrogenation with standard reaction conditions (see the Supporting Information, Scheme S1).

https://doi.org/10.1021/acsomega.2c01566
ACS Omega 2022, 7, 19804−19815

Green Chemistry Metrics for the Hydrogenation of 4-Nitrobenzamide and Benzaldehyde. In line with the Sustainable Development Goals (SDGs), it is highly important to measure the merits and demerits of chemical processes by following the guidelines of 12 principles of green chemistry.[58] To measure the sustainable and green credentials, we adopted the CHEM21 green metrics toolkit developed by Clark and co-workers.[59] In this respect, we have chosen two different hydrogenation reactions that worked efficiently under standard reaction conditions, and the corresponding results are summarized in Table 3. In both the cases, yield, conversion, and selectivity were assessed using an isolated yield of products, and purity was determined using NMR. Reactions A and B ended up with full conversion and afforded quantitative selectivity and yield. Hence, these reactions (A and B) receive green flags for yield, conversion, and selectivity. The atom economy and reaction mass efficiency for reaction A are 79.09 and 75.58%, whereas the atom economy and reaction mass efficiency for reaction B are 100 and 95%, respectively. As we used THF and water as solvents in 10:1 ratio for reactions A and B, we received an amber flag. Iron is used as a catalyst in both the reactions (A and B) and received a green flag considering the abundance and toxicity of the element. As we conducted the hydrogenation reactions A and B in batch mode and not in a continuous process, the amber flag was received. Simple workup techniques such as filtration and evaporation were implemented in reactions A and B and therefore earned a green flag. All of the hydrogenation reactions were conducted at 120 °C, so it obtained an amber flag under energy. Reactions A and B do not have any health and safety issues, and therefore, they get green flags. Overall, the assessment of selected reactions A and B indicates that the chemical process is green and eco-friendly.

CONCLUSIONS

In conclusion, an inexpensive and sustainable magnetically recoverable γ-Fe_2O_3/LRC-700 nanocatalyst has been successfully prepared by the hydrothermal treatment, followed by the impregnation and pyrolysis method. The as-prepared γ-Fe_2O_3/LRC-700 nanocatalyst displayed excellent selectivity and activity for the hydrogenation of functionalized and challenging nitroarenes, including pharmaceuticals, to the corresponding anilines in high yields. Additionally, the γ-Fe_2O_3/LRC-700 nanocatalyst is also extremely active for the hydrogenation of biomass-derived furfuraldehyde and other aromatic aldehydes using molecular hydrogen as a reducing agent. The exceptional activity of the γ-Fe_2O_3/LRC-700 nanocatalyst is due to benefiting the combination of lignin residue and urea, resulting in γ-Fe_2O_3 nanoparticles with a small size in the range of 2−7 nm and strong interaction between N atoms and Fe nanoparticles, which leads to highly stable γ-Fe_2O_3 nanoparticles. Furthermore, the γ-Fe_2O_3/LRC-700 nanocatalyst can be easily separated by an external magnet and reused for five catalytic runs with no significant drop in the catalytic activity. Finally, the atom economy and reaction mass efficiency for the hydrogenation of 4-nitrobenzamide to 4-aminobenzamide are 79.09 and 75.58% whereas for the reduction of benzaldehyde to benzyl alcohol is 100 and 95% respectively, which represents the sustainable and green credentials of the reactions, evaluated with the help of the CHEM21 green metrics toolkit.

ASSOCIATED CONTENT

Supporting Information

The Supporting Information is available free of charge at https://pubs.acs.org/doi/10.1021/acsomega.2c01566.

General considerations, unsuccessful aliphatic aldehydes, survey XPS spectrum of the fresh Fe/LRC-700 nanocatalyst, XPS spectrum of the spent Fe/LRC-700 nanocatalyst, survey XPS spectrum of the spent Fe/LRC-700 nanocatalyst, ^{1}H and ^{13}C NMR spectral data of amines and alcohols, and copies of ^{1}H and ^{13}C NMR and GC−MS of amines and alcohols (PDF)

AUTHOR INFORMATION

Corresponding Authors

Kishore Natte − *Department of Chemistry, Indian Institute of Technology (IIT) Hyderabad, Kandi 502285 Telangana, India;* orcid.org/0000-0001-8557-1969; Email: kishore.natte@chy.iith.ac.in, kishorenatte@gmail.com

Anand Narani − *Biofuels Division, CSIR-Indian Institute of Petroleum, Dehradun 248005, India; Academy of Scientific and Innovative Research (AcSIR), Ghaziabad 201002 Uttar Pradesh, India;* orcid.org/0000-0003-2760-3429; Email: anand.narani@iip.res.in, naranialr1@gmail.com

Authors

Naina Sarki − *Chemical and Material Sciences Division, CSIR-Indian Institute of Petroleum, Dehradun 248005, India; Academy of Scientific and Innovative Research (AcSIR), Ghaziabad 201002 Uttar Pradesh, India;* orcid.org/0000-0002-6779-3039

Raju Kumar − *Biofuels Division, CSIR-Indian Institute of Petroleum, Dehradun 248005, India; Academy of Scientific and Innovative Research (AcSIR), Ghaziabad 201002 Uttar Pradesh, India*

Baint Singh − *Biofuels Division, CSIR-Indian Institute of Petroleum, Dehradun 248005, India; Academy of Scientific and Innovative Research (AcSIR), Ghaziabad 201002 Uttar Pradesh, India*

Anjan Ray − *Analytical Sciences Division, CSIR-Indian Institute of Petroleum, Dehradun 248005, India; Academy of Scientific and Innovative Research (AcSIR), Ghaziabad 201002 Uttar Pradesh, India;* orcid.org/0000-0003-0547-9017

Ganesh Naik − *Analytical Sciences Division, CSIR-Indian Institute of Petroleum, Dehradun 248005, India; Academy of Scientific and Innovative Research (AcSIR), Ghaziabad 201002 Uttar Pradesh, India*

Complete contact information is available at: https://pubs.acs.org/10.1021/acsomega.2c01566

Notes

The authors declare no competing financial interest.

ACKNOWLEDGMENTS

K.N. acknowledges DST-SERB, New Delhi (SRG/2019/002004), for financial support. N.S. and R.K. are thankful to Council of Scientific and Industrial Research (CSIR), New Delhi, for awarding fellowship. B.S. is thankful to DST-Inspire for awarding a research fellowship. The authors are thankful to the analytical staff of CSIR-IIP, Dehradun, for their excellent support.

REFERENCES

(1) Weissermel, K. A.et al. *Industrial Organic Chemistry*, 4th ed.; Wiley-VCH, 2008.

(2) Jagadeesh, R. V.; Surkus, A.-E.; Junge, H.; Pohl, M.-M.; Radnik, J.; Rabeah, J.; Huan, H.; Schünemann, V.; Brückner, A.; Beller, M. Nanoscale Fe_2O_3-Based Catalysts for Selective Hydrogenation of Nitroarenes to Anilines. *Science* **2013**, *342*, 1073−1076.

(3) Liu, W.; Li, W.; Spannenberg, A.; Junge, K.; Beller, M. Iron-catalysed regioselective hydrogenation of terminal epoxides to alcohols under mild conditions. *Nat. Catal.* **2019**, *2*, 523−528.

(4) Formenti, D.; Ferretti, F.; Scharnagl, F. K.; Beller, M. Reduction of Nitro Compounds Using 3d-Non-Noble Metal Catalysts. *Chem. Rev.* **2019**, *119*, 2611−2680.

(5) *Common Fragrance and Flavor Materials* Surburg, H. P. J., Ed.; Wiley-VCH: Weinheim, Germany, 2006.

(6) Murugesan, K.; Senthamarai, T.; Chandrashekhar, V. G.; Natte, K.; Kamer, P. C. J.; Beller, M.; Jagadeesh, R. V. Catalytic reductive aminations using molecular hydrogen for synthesis of different kinds of amines. *Chem. Soc. Rev.* **2020**, *49*, 6273−6328.

(7) Cabrero-Antonino, J. R.; Adam, R.; Papa, V.; Beller, M. Homogeneous and heterogeneous catalytic reduction of amides and related compounds using molecular hydrogen. *Nat. Commun.* **2020**, *11*, No. 3893.

(8) Carvalho, R. L.; de Miranda, A. S.; Nunes, M. P.; Gomes, R. S.; Jardim, G. A. M.; Júnior, E. N. S. On the application of 3d metals for C−H activation toward bioactive compounds: The key step for the synthesis of silver bullets. *Beilstein J. Org. Chem.* **2021**, *17*, 1849−1938.

(9) Gandeepan, P.; Müller, T.; Zell, D.; Cera, G.; Warratz, S.; Ackermann, L. 3d Transition Metals for C−H Activation. *Chem. Rev.* **2019**, *119*, 2192−2452.

(10) Liu, L.; Corma, A. Metal Catalysts for Heterogeneous Catalysis: From Single Atoms to Nanoclusters and Nanoparticles. *Chem. Rev.* **2018**, *118*, 4981−5079.

(11) Frey, P. A.; Reed, G. H. The Ubiquity of Iron. *ACS Chem. Biol.* **2012**, *7*, 1477−1481.

(12) Chandrashekhar, V. G.; Senthamarai, T.; Kadam, R. G.; Malina, O.; Kašlík, J.; Zbořil, R.; Gawande, M. B.; Jagadeesh, R. V.; Beller, M. Silica-supported Fe/Fe−O nanoparticles for the catalytic hydrogenation of nitriles to amines in the presence of aluminium additives. *Nat. Catal.* **2022**, *5*, 20−29.

(13) Corma, A.; Serna, P. Chemoselective Hydrogenation of Nitro Compounds with Supported Gold Catalysts. *Science* **2006**, *313*, 332−334.

(14) Orlandi, M.; Brenna, D.; Harms, R.; Jost, S.; Benaglia, M. Recent Developments in the Reduction of Aromatic and Aliphatic Nitro Compounds to Amines. *Org. Process Res. Dev.* **2018**, *22*, 430−445.

(15) Natte, K.; Jagadeesh, R. V. Amines By Reduction. In *Kirk−Othmer Encyclopedia of Chemical Technology*, Wiley, 2000; pp 1−34.

(16) Goyal, V.; Sarki, N.; Natte, K.; Ray, A. Pd/C-catalyzed transfer hydrogenation of aromatic nitro compounds using methanol as a hydrogen source. *J. Indian Chem. Soc.* **2021**, *98*, No. 100014.

(17) Westerhaus, F. A.; Jagadeesh, R. V.; Wienhöfer, G.; Pohl, M.-M.; Radnik, J.; Surkus, A.-E.; Rabeah, J.; Junge, K.; Junge, H.; Nielsen, M.; Brückner, A.; Beller, M. Heterogenized cobalt oxide catalysts for nitroarene reduction by pyrolysis of molecularly defined complexes. *Nat. Chem.* **2013**, *5*, 537−543.

(18) Zhou, P.; Jiang, L.; Wang, F.; Deng, K.; Lv, K.; Zhang, Z. High performance of a cobalt-nitrogen complex for the reduction and reductive coupling of nitro compounds into amines and their derivatives. *Sci. Adv.* **2017**, *3*, No. e1601945.

(19) Eckardt, M.; Zaheer, M.; Kempe, R. Nitrogen-doped mesoporous SiC materials with catalytically active cobalt nanoparticles for the efficient and selective hydrogenation of nitroarenes. *Sci. Rep.* **2018**, *8*, No. 2567.

(20) Goswami, A.; Kadam, R. G.; Tuček, J.; Sofer, Z.; Bouša, D.; Varma, R. S.; Gawande, M. B.; Zbořil, R. Fe(0)-embedded thermally reduced graphene oxide as efficient nanocatalyst for reduction of nitro compounds to amines. *Chem. Eng. J.* **2020**, *382*, No. 122469.

(21) Lam, E.; Luong, J. H. T. Carbon Materials as Catalyst Supports and Catalysts in the Transformation of Biomass to Fuels and Chemicals. *ACS Catal.* **2014**, *4*, 3393−3410.

(22) Abdullah, S. H. Y. S.; Hanapi, N. H. M.; Azid, A.; Umar, R.; Juahir, H.; Khatoon, H.; Endut, A. A review of biomass-derived heterogeneous catalyst for a sustainable biodiesel production. *Renewable Sustainable Energy Rev.* **2017**, *70*, 1040−1051.

(23) Varma, R. S. Biomass-Derived Renewable Carbonaceous Materials for Sustainable Chemical and Environmental Applications. *ACS Sustainable Chem. Eng.* **2019**, *7*, 6458−6470.

(24) Veerakumar, P.; Panneer Muthuselvam, I.; Hung, C.-T.; Lin, K.-C.; Chou, F.-C.; Liu, S.-B. Biomass-Derived Activated Carbon Supported Fe_3O_4 Nanoparticles as Recyclable Catalysts for Reduction of Nitroarenes. *ACS Sustainable Chem. Eng.* **2016**, *4*, 6772−6782.

(25) Song, T.; Li, Q.; Ma, Z.; Yang, Y. Recent advance in selective hydrogenation reaction catalyzed by biomass-derived non-noble metal nanocomposites. *Tetrahedron Lett.* **2021**, *83*, No. 153331.

(26) Song, T.; Ren, P.; Duan, Y.; Wang, Z.; Chen, X.; Yang, Y. Cobalt nanocomposites on N-doped hierarchical porous carbon for highly selective formation of anilines and imines from nitroarenes. *Green Chem.* **2018**, *20*, 4629−4637.

(27) Duan, Y.; Dong, X.; Song, T.; Wang, Z.; Xiao, J.; Yuan, Y.; Yang, Y. Hydrogenation of Functionalized Nitroarenes Catalyzed by Single-Phase Pyrite FeS2 Nanoparticles on N,S-Codoped Porous Carbon. *ChemSusChem* **2019**, *12*, 4636−4644.

(28) Goyal, V.; Sarki, N.; Singh, B.; Ray, A.; Poddar, M.; Bordoloi, A.; Narani, A.; Natte, K. Carbon-Supported Cobalt Nanoparticles as Catalysts for the Selective Hydrogenation of Nitroarenes to Arylamines and Pharmaceuticals. *ACS Appl. Nano Mater.* **2020**, *3*, 11070−11079.

(29) Goyal, V.; Sarki, N.; Poddar, M. K.; Narani, A.; Tripathi, D.; Ray, A.; Natte, K. Biorenewable carbon-supported Ru catalyst for N-alkylation of amines with alcohols and selective hydrogenation of nitroarenes. *New J. Chem.* **2021**, *45*, 14687−14694.

(30) Kumar, A.; Goyal, V.; Sarki, N.; Singh, B.; Ray, A.; Bhaskar, T.; Bordoloi, A.; Narani, A.; Natte, K. Biocarbon Supported Nanoscale Ruthenium Oxide-Based Catalyst for Clean Hydrogenation of Arenes and Heteroarenes. *ACS Sustainable Chem. Eng.* **2020**, *8*, 15740−15754.

(31) Gorgas, N.; Stöger, B.; Veiros, L. F.; Kirchner, K. Highly Efficient and Selective Hydrogenation of Aldehydes: A Well-Defined Fe(II) Catalyst Exhibits Noble-Metal Activity. *ACS Catal.* **2016**, *6*, 2664−2672.

(32) Nakagawa, Y.; Tamura, M.; Tomishige, K. Catalytic Reduction of Biomass-Derived Furanic Compounds with Hydrogen. *ACS Catal.* **2013**, *3*, 2655−2668.

(33) Luneau, M.; Lim, J. S.; Patel, D. A.; Sykes, E. C. H.; Friend, C. M.; Sautet, P. Guidelines to Achieving High Selectivity for the Hydrogenation of α,β-Unsaturated Aldehydes with Bimetallic and Dilute Alloy Catalysts: A Review. *Chem. Rev.* **2020**, *120*, 12834−12872.

(34) Saudan, L. A. Hydrogenation Processes in the Synthesis of Perfumery Ingredients. *Acc. Chem. Res.* **2007**, *40*, 1309−1319.

(35) Suresh Kumar, B.; Puthiaraj, P.; Amali, A. J.; Pitchumani, K. Ultrafine Bimetallic PdCo Alloy Nanoparticles on Hollow Carbon Capsules: An Efficient Heterogeneous Catalyst for Transfer Hydrogenation of Carbonyl Compounds. *ACS Sustainable Chem. Eng.* **2018**, *6*, 491−500.

(36) Bonomo, L.; Kermorvan, L.; Dupau, P. Ruthenium-Catalyzed Highly Chemoselective Hydrogenation of Aldehydes. *ChemCatChem* **2015**, *7*, 907−910.

(37) Natte, K.; Li, W.; Zhou, S.; Neumann, H.; Wu, X.-F. Iron-catalyzed reduction of aromatic aldehydes with paraformaldehyde and H_2O as the hydrogen source. *Tetrahedron Lett.* **2015**, *56*, 1118−1121.

(38) Chakraborty, S.; Bhattacharya, P.; Dai, H.; Guan, H. Nickel and Iron Pincer Complexes as Catalysts for the Reduction of Carbonyl Compounds. *Acc. Chem. Res.* **2015**, *48*, 1995−2003.

(39) Yang, W.; Chernyshov, I. Y.; van Schendel, R. K. A.; Weber, M.; Müller, C.; Filonenko, G. A.; Pidko, E. A. Robust and efficient

https://doi.org/10.1021/acsomega.2c01566
ACS Omega 2022, 7, 19804−19815

hydrogenation of carbonyl compounds catalysed by mixed donor Mn(I) pincer complexes. *Nat. Commun.* **2021**, *12*, No. 12.
(40) Glatz, M.; Stöger, B.; Himmelbauer, D.; Veiros, L. F.; Kirchner, K. Chemoselective Hydrogenation of Aldehydes under Mild, Base-Free Conditions: Manganese Outperforms Rhenium. *ACS Catal.* **2018**, *8*, 4009−4016.
(41) Zhu, Y.; Li, Z.; Chen, J. Applications of lignin-derived catalysts for green synthesis. *Green Energy Environ.* **2019**, *4*, 210−244.
(42) Li, C.; Zhao, X.; Wang, A.; Huber, G. W.; Zhang, T. Catalytic Transformation of Lignin for the Production of Chemicals and Fuels. *Chem. Rev.* **2015**, *115*, 11559−11624.
(43) Natte, K.; Narani, A.; Goyal, V.; Sarki, N.; Jagadeesh, R. V. Synthesis of Functional Chemicals from Lignin-derived Monomers by Selective Organic Transformations. *Adv. Synth. Catal.* **2020**, *362*, 5143−5169.
(44) Liu, W.; You, W.; Sun, W.; Yang, W.; Korde, A.; Gong, Y.; Deng, Y. Ambient-pressure and low-temperature upgrading of lignin bio-oil to hydrocarbons using a hydrogen buffer catalytic system. *Nat. Energy* **2020**, *5*, 759−767.
(45) Rawat, S.; Singh, B.; Kumar, R.; Pendem, C.; Bhandari, S.; Natte, K.; Narani, A. Value addition of lignin to zingerone using recyclable $AlPO_4$ and Ni/LRC catalysts. *Chem. Eng. J.* **2022**, *431*, No. 134130.
(46) Anand, N.; Reddy, K. H. P.; Satyanarayana, T.; Rao, K. S. R.; Burri, D. R. A magnetically recoverable γ-Fe_2O_3 nanocatalyst for the synthesis of 2-phenylquinazolines under solvent-free conditions. *Catal. Sci. Technol.* **2012**, *2*, 570−574.
(47) Woo, K.; Hong, J.; Choi, S.; Lee, H.-W.; Ahn, J.-P.; Kim, C. S.; Lee, S. W. Easy Synthesis and Magnetic Properties of Iron Oxide Nanoparticles. *Chem. Mater.* **2004**, *16*, 2814−2818.
(48) Cui, X.; Surkus, A.-E.; Junge, K.; Topf, C.; Radnik, J.; Kreyenschulte, C.; Beller, M. Highly selective hydrogenation of arenes using nanostructured ruthenium catalysts modified with a carbon−nitrogen matrix. *Nat. Commun.* **2016**, *7*, No. 11326.
(49) Yu, J.; Chen, G.; Sunarso, J.; Zhu, Y.; Ran, R.; Zhu, Z.; Zhou, W.; Shao, Z. Cobalt Oxide and Cobalt-Graphitic Carbon Core−Shell Based Catalysts with Remarkably High Oxygen Reduction Reaction Activity. *Adv. Sci.* **2016**, *3*, No. 1600060.
(50) Cao, D.; Li, H.; Pan, L.; Li, J.; Wang, X.; Jing, P.; Cheng, X.; Wang, W.; Wang, J.; Liu, Q. High saturation magnetization of γ-Fe2O3 nano-particles by a facile one-step synthesis approach. *Sci. Rep.* **2016**, *6*, No. 32360.
(51) Ma, D.; Veres, T.; Clime, L.; Normandin, F.; Guan, J.; Kingston, D.; Simard, B. Superparamagnetic FexOy@SiO_2 Core−Shell Nanostructures: Controlled Synthesis and Magnetic Characterization. *J. Phys. Chem. C* **2007**, *111*, 1999−2007.
(52) Fujii, T.; de Groot, F. M. F.; Sawatzky, G. A.; Voogt, F. C.; Hibma, T.; Okada, K. In situ XPS analysis of various iron oxide films grown by NO_2-assisted molecular-beam epitaxy. *Phys. Rev. B* **1999**, *59*, 3195−3202.
(53) Geng, Z.; Lin, Y.; Yu, X.; Shen, Q.; Ma, L.; Li, Z.; Pan, N.; Wang, X. Highly efficient dye adsorption and removal: a functional hybrid of reduced graphene oxide−Fe3O4 nanoparticles as an easily regenerative adsorbent. *J. Mater. Chem.* **2012**, *22*, 3527−3535.
(54) Wu, G.; More, K. L.; Johnston, C. M.; Zelenay, P. High-Performance Electrocatalysts for Oxygen Reduction Derived from Polyaniline, Iron, and Cobalt. *Science* **2011**, *332*, 443−447.
(55) Blaser, H.-U.; Steiner, H.; Studer, M. Selective Catalytic Hydrogenation of Functionalized Nitroarenes: An Update. *ChemCatChem* **2009**, *1*, 210−221.
(56) Chandrashekhar, V. G.; Natte, K.; Alenad, A. M.; Alshammari, A. S.; Kreyenschulte, C.; Jagadeesh, R. V. Reductive Amination, Hydrogenation and Hydrodeoxygenation of 5-Hydroxymethylfurfural using Silica-supported Cobalt- Nanoparticles. *ChemCatChem* **2022**, *14*, No. e202101234.
(57) Wang, Y.; Zhao, D.; Rodríguez-Padrón, D.; Len, C. Recent Advances in Catalytic Hydrogenation of Furfural. *Catalysts* **2019**, *9*, 796.
(58) Anastas, P.; Eghbali, N. Green Chemistry: Principles and Practice. *Chem. Soc. Rev.* **2010**, *39*, 301−312.
(59) McElroy, C. R.; Constantinou, A.; Jones, L. C.; Summerton, L.; Clark, J. H. Towards a holistic approach to metrics for the 21st century pharmaceutical industry. *Green Chem.* **2015**, *17*, 3111−3121.

https://doi.org/10.1021/acsomega.2c01566
ACS Omega 2022, 7, 19804−19815